Journal Pre-proof

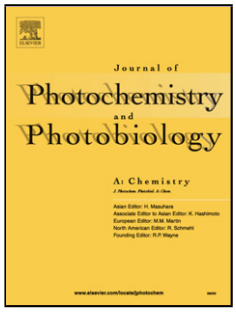

Hydroxy-Benzimidazoles as Blue-Green Emitters: Synthesis, Structural and DFT Studies

Reshma Sathyanarayana, Vasantha Kumar, G H Pujar, Boja Poojary, Madan Kumar Shankar, Sangappa Yallappa

PII: S1010-6030(20)30550-5

DOI: https://doi.org/10.1016/j.jphotochem.2020.112751

Reference: JPC 112751

To appear in: *Journal of Photochemistry & Photobiology, A: Chemistry*

Received Date: 29 February 2020

Revised Date: 27 June 2020

Accepted Date: 4 July 2020

Please cite this article as: Sathyanarayana R, Kumar V, H Pujar G, Poojary B, Shankar MK, Yallappa S, Hydroxy-Benzimidazoles as Blue-Green Emitters: Synthesis, Structural and DFT Studies, *Journal of Photochemistry and amp; Photobiology, A: Chemistry* (2020), doi: https://doi.org/10.1016/j.jphotochem.2020.112751

Hydroxy-Benzimidazoles as Blue-Green Emitters: Synthesis, Structural and DFT Studies

Reshma Sathyanarayana[a], Vasantha Kumar[b], G H Pujar[c], Boja Poojary[a,*], Madan Kumar Shankar[d], Sangappa Yallappa[e]

[a]*Department of Chemistry, Mangalore University, Mangalagangothri-574199, Karnataka, India. E-Mail: bojapoojary@gmail.com. Tel.: +91 824 2287262; Fax: +91 824 2287367;*

[b]*Department of Chemistry, Sri Dharmasthala Manjunatheshwara College (Autonomous), Ujire, Karanataka – 574240;*

[c]*Research Centre, Department of Physics, GM Institute of Technology, Davangere, Karnataka, India-577006*

[d]*IOE, Vijnana Bhavan, University of Mysore, Mysuru, India 570006*

[e] *Department of Physics, Mangalore University, Mangalagangothri-574199, Karnataka, India.*

Highlights

- Five novel bipolar benzimidazole derivatives (**3a-e**) were synthesized *via* "one-pot" nitro reductive cyclization as blue-green fluorescent emitters.
- Simple and cost-effective synthetic routes. Products obtained with high yield.
- All derivatives exhibited high stokes effect, high to moderate quantum yield and good thermal stability.
- All the derivatives exhibit ESIPT process
- Computational studies like DFT, MEP were studied

Abstract

The new benzimidazole ligands (**3a-e)** were synthesized using ethyl 4-(butylamino)-3-nitrobenzoate and substituted salicylaldehyde in the presence of sodium dithionite reagent which undergoes "one-pot'' nitro reductive cyclization. Here benzimidazole moiety acts as an electron-acceptor (A) whereas substituted 2-hydroxyphenyl moiety acts as an electron-donor (D) unit. The molecular structures were characterised by FTIR, ^{1}H NMR, ^{13}C NMR, single crystal XRD and MS analysis. Optoelectronic properties were determined by UV-vis, solution and solid photoluminescence, quantum yield and lifetime. The solvent-dependent absorption and emission were studied using both polar protic and polar aprotic solvents. All the derivatives exhibited ESIPT, especially compound ethyl 1-butyl-2-(3,5-dichloro-2-hydroxyphenyl)-1*H*-benzo[*d*]imidazole-5-carboxylate (**3e**) displayed dual emission in both polar protic and polar

aprotic solvents. The compound stability and electrochemical property were determined by thermal gravimetric analysis (TGA) and cyclic voltammetry (CV) respectively. The compounds emit intense blue-green fluorescence with high to moderate quantum yield. Also, these derivatives exhibited a high Stokes shift. The computational studies like Density-Functional Theory (DFT) and Molecular Electrostatic Potential (MEP) were conducted to provide important insights into the structure-property relationships. The crystal packing is stabilized through intermolecular hydrogen bonds (C---H...O) and intermolecular interactions ($\pi\ldots\ \pi$). The findings of results help in developing novel ligands in the field of organic optoelectronics.

Key words: Benzimidazole; Photoluminescence; DFT; Cyclic voltammetry; MEP; Quantum yield; Fluorescence lifetime; ESIPT

Introduction

Before organic light-emitting diodes (OLEDs) came to light, various display technologies such as inorganic light-emitting diodes, liquid crystal displays, plasma displays and cathode ray tubes were top in the market. Due to many drawbacks of these display technologies, OLEDs emerged in present generation display technology with superior characteristics to overcome the limitations like colour tunability, bulkiness and low viewing angle [1]. OLEDs are thin, flat with large surface area, lightweight, flexible and bendable. It is possible to attain unbroken light emission over a large surface area due to the organic nature of OLEDs. Energy saving, low weight, brightness, reduction in thickness, large viewing angle, reduction in cost, colour reproduction and low power consumption are some of the key advantages of OLEDs [2]. These have also emerged in the field of commercial products such as digital cameras and cell phones [3]. Hence a great deal of work has been carried out in the development of visible light-emitting OLEDs. The efficacy of fluorophores boosted when they undergo excited state intramolecular proton transfer (ESIPT) [4, 5]. The molecules exhibiting ESIPT process have been used as polymer photo-stabilizer [6], fluorescent probes [7], laser dyes [8] and light-emitting materials for electroluminescent devices [9].

One of the major problems faced by the organic and polymer chromophore is the high emission property in dilute solution but weak luminescent in solid state [10]. This is due to the aggregation-caused quenching (ACQ), where aggregation of molecules takes place resulting in less emission. But, for the practical applications luminophores should exist in solid films. Henceforth, few researchers worked on aggregation-induced emission (AIE), which is the

opposite of ACQ where molecules will be luminesce in aggregation state rather than in solution state [11-13].

Apart from benzimidazole moiety being a bioactive molecule in the pharmaceutical field [14-18], this moiety was also found to display exciting fluorescent and photophysical properties [19-21]. One of the best methods to enhance fluorescence properties, device efficiency and operational lifetime is to incorporate donor/acceptor strategy. This in turn depends on the number of holes (HT) and electron transporting (ET) moieties [22, 23]. The electroluminescent materials with high emission quantum yield, high glass-transition temperature and balance of holes and electrons are successfully employed in single-layer OLEDs [24]. The design and synthesis of small bipolar molecules combining both electron-donating and electron-withdrawing groups in the same molecule enhance the fluorescence efficiency. Electron-donating moieties such as carbazole and diphenylamine act as a hole-transporting component whereas electron-withdrawing moieties such as benzimidazole, 1,3,4-oxadiazole, phosphine oxide and triazine behave as electron – transporting acceptors [25].

Benzimidazole also played a significant role in the field of coordination chemistry as this moiety is capable of forming stable complexes with metal ions. Due to the presence of a high electron density zone, benzimidazole also behaves as a corrosion inhibitor [26]. This moiety also made an impact in the field of flame retardants, liquid materials, CO_2 chemosensors and supramolecular chemistry [27].

Given these findings, novel bipolar benzimidazole derivatives **3a-e** as blue-green emitting fluorescent material have been synthesized by inserting benzimidazole as an electron acceptor (A) and substituted 2-hydroxyphenyl as an electron-donor (D) unit (**Fig. 1.**). The combination of electron-donating and electron-withdrawing in the single molecular framework results in strong intramolecular charge transfer. The blue-emitting fluorescent material can be used both as blue-emitting OLEDs as well as host for white and other colours [28]. The optoelectronic properties such as UV-vis/fluorescence spectra; thermal property like thermogravimetric analysis (TGA); computational studies such as HOMO-LUMO calculations and molecular electrostatic potential (MEP); electrochemical property by cyclic voltammetry (CV) have been studied and analysed. Furthermore, the solvatochromic behaviour of the title compounds was examined to study the strong intramolecular charge transfer. In addition, quantum yield and fluorescence lifetime of the derivatives were also studied. The findings of these studies help in discovering suitable OLEDs.

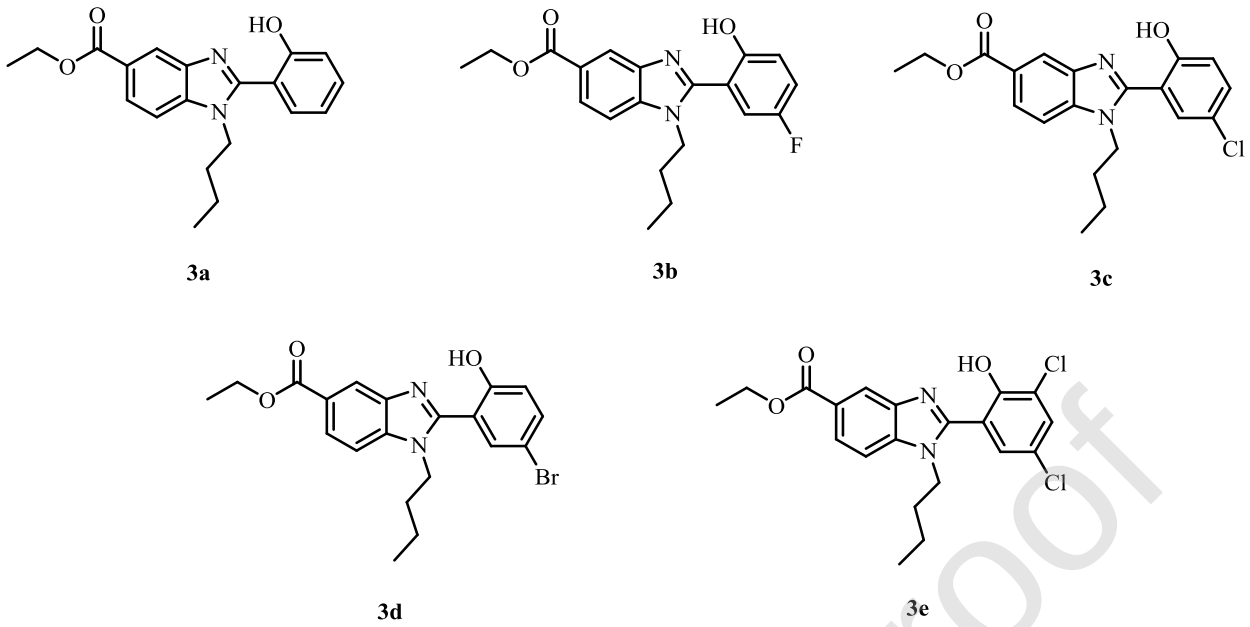

Fig. 1: Chemical structures of synthesized target molecules **3a-e**

Experimental

Materials and methods

The reagents used for the synthesis of this series were analytical grade and purchased from S. D. Fine, Sigma-Aldrich and Spectrochem, which were used directly without further purification. Only the analytical solvents were used during the experiments. The completion of the reaction was determined by thin-layer chromatography plate from Merck. Recrystallization was used as a purification method either in dimethylformamide or ethanol as a solvent.

Procedure for the synthesis of ethyl-4-chloro-3-nitrobenzoate (1)

To a solution of 4-chloro-3-nitrobenzoic acid (10 g, 49.6 mmol) in ethanol (100 mL) added a catalytic amount of conc. H_2SO_4 and heated to reflux for 16 h. The completion of the reaction was monitored by TLC. After the completion of the reaction, excess of solvent was removed under high vacuum and the residue was poured into ice-cold water. The precipitate formed was filtered and dried to afford intermediate **1** as white solid. Yield: 92%

Procedure for the synthesis of ethyl 4-(butylamino)-3-nitrobenzoate (2)

Ethyl-4-chloro-3-nitrobenzoate (10.5 g, 45.8 mmol) was taken in dry THF. To this mixture butylamine (45.8 mmol) and TEA (45.8 mmol) were added at room temperature and stirred

overnight at the same temperature. The completion of the reaction was monitored by thin-layer chromatography. Excess of solvent was removed under a high vacuum and the residue left was added into ice-cold water. The precipitate formed was filtered, dried and recrystallized from ethanol to yield intermediate **2** as yellow solid. Yield: 82%

Yellow solid; Yield: 82%; M.p.: 70-72 °C; ^{1}H NMR (400 MHz, DMSO-d_6, δ ppm): 0.98-1.019 (t, 3H, J = 12 Hz, 4-CH_3), 1.37-1.40 (t, 3H, *J* = 12 Hz, ester CH_3) 1.46-1.52 (quint, 2H, 3-CH_2), 1.70-1.76 (quint, 2H, 2-CH_2), 3.33-3.38 (q, 2H, *J* = 4 Hz, ester CH_2) 4.33-4.38 (t, 2H, 1-CH_2), 6.85-6.87 (d, 1H, *J* = 8 Hz, H_5 of benzyl), 8.061-8.067 (d, 1H, *J* = 2.4 Hz, H_6 of benzyl), 8.33 (bs, 1H, NH), 8.872-8.877 (d, 1H, *J* = 2 Hz, H_2 of benzyl) ppm; ^{13}C NMR (100 MHz): δ = 165.4, 147.9, 136.5, 131.3, 129.6, 117.5, 113.6, 61.2, 43.1, 31.08, 20.3, 14.5, 13.9; MS: calculated for $C_{13}H_{18}N_2O_4$ is 266.13; found $[M+H]^+$ 267.15 *m/z*; Anal. calcd. for $C_{13}H_{18}N_2O_4$: C, 58.63; H, 6.81; N, 10.52%. Found: C, 58.60; H, 6.79; N, 10.50%.

General procedure for the synthesis of ethyl 1-butyl-2-(2-hydroxyphenyl)-1H-benzo[d]imidazole-5-carboxylate (3a-e)

To a stirred solution of intermediate **2** (0.5 g, 19.8 mmol) in dry DMSO (5 mL), substituted salicylaldehyde (19.8 mmol) and sodium dithionite (39.6 mmol) was added and heated to 90 °C with stirring for 3 h. After completion of the reaction, the reaction mass was poured into ice-cold water. The precipitate formed was filtered, dried and recrystallized from DMF to afford the target compound **3a-e**. Yield: 90-95%.

Ethyl 1-butyl-2-(2-hydroxyphenyl)-1H-benzo[d]imidazole-5-carboxylate (3a)

Off white solid; yield: 92%; melting point (°C): 98-100; FT IR (ATR, υ_{max}/cm): 3477 (-OH), 1701 (C=O of ester), 1292 (C-O of ester). ^{1}H NMR (400 MHz, DMSO-d_6): δ = 0.99-1.03 (t, 3H, *J* = 16 Hz, 4-CH_3), 1.44-1.50 (m, 5H, ester CH_3 and 3-CH_2), 1.93-2.01 (quint, 2H, 2-CH_2), 4.39-4.45 (q, 4H, *J* = 8 Hz, ester CH_2 and 1-CH_2), 6.96-6.99 (m, 1H, H_3 of 2-hydroxy-phenyl) 7.15-7.17 (d, 1H, *J* = 8 Hz, H_5 of 2-hydroxy-phenyl), 7.36-7.44 (m, 1H, H_4, H_6 of 2-hydroxy-phenyl), 7.61-7.63 (d, 1H, *J* = 8 Hz, H_6 of benzimidazole), 8.05-8.07 (d, 1H, *J* = 8 Hz, H_7 of benzimidazole), 8.47 (s, 1H, H_4 benzimidazole) ppm; ^{13}C NMR (100 MHz): δ = 13.8, 14.6, 20.2, 32.0, 46.0, 61.2, 109.7, 113.0, 118.6, 119.0, 121.2, 125.0, 125.7, 126.7, 132.1, 138.4, 140.2, 153.0, 159.3, 167.0 ppm; MS: calculated for $C_{20}H_{22}N_2O_3$ is 338.16; found $[M+H]^+$ 339.05 *m/z*; Anal.calc. for $C_{20}H_{22}N_2O_3$: C, 70.99; H, 6.55; N, 8.28%. Found: C, 70.95; H, 6.53; N, 8.20%; Uv-Vis: λ_{max} (ACN) = 322 nm, Fluorescence: λ_{ex} = 322 nm, λ_{em} (ACN) = 474 nm, Φ = 0.14.

Ethyl 1-butyl-2-(5-fluoro-2-hydroxyphenyl)-1H-benzo[d]imidazole-5-carboxylate (3b)

Off white solid; yield: 90%; melting point (°C): 146-148; FT IR (ATR, υ_{max}/cm): 3412 (-OH), 1715 (C=O of ester), 1021 (C-F), 1215 (C-O of ester); ^{1}H NMR (400 MHz, DMSO-d_6): δ = 1.007-1.04 (t, 3H, *J* = 13 Hz, 4-CH_3), 1.42-1.47 (m, 5H, ester CH_3 and 3-CH_2), 1.95-1.99 (quint, 2H, 2-CH_2), 4.40-4.45 (q, 4H, *J* = 8 Hz, ester CH_2 and 1-CH_2), 7.10-7.12 (dd, 2H, H_3 and H_4 of 5-fluoro-2-hydroxyphenyl), 7.32-7.35 (m, H_7 of benzimidazole), 7.43-7.45 (d, 1H, *J* = 8 Hz, H_8 of benzimidazole), 8.07-8.073 (dd, 1H, *J* = 1.2 Hz, H_5 of benzimidazole), 8.472-8.474 (d, 1H, *J* = 0.8 Hz, H_6 of 5-fluoro-2-hydroxyphenyl) ppm; ^{13}C NMR (100 MHz): δ = 13.7, 14.6, 20.2, 32.0, 45.9, 61.2, 109.8, 112.7, 112.75 (J = 40 Hz), 119.0 (*J* = 92 Hz), 119.6 (*J* = 32 Hz), 121.4, 125.3, 126.0, 138.3, 140.0, 152.0, 154.3, 156.1 (*J* = 480 Hz), 166.94 ppm; MS: calculated for $C_{20}H_{21}N_2FO_3$ is 356.15; found $[M+H]^+$ 357.10 *m/z*; Anal.calc. for $C_{20}H_{21}N_2FO_3$: C, 67.40; H, 5.94; N, 7.86%. Found: C, 67.3; H, 5.90; N, 7.50%; Uv-Vis: λ_{max} (ACN) = 332 nm, Fluorescence: λ_{ex} = 332 nm, λ_{em} (ACN) = 487 nm, Φ = 0.03.

Ethyl 1-butyl-2-(5-chloro-2-hydroxyphenyl)-1H-benzo[d]imidazole-5-carboxylate (3c)

Off white solid; yield: 95%; melting point (°C): 120-122; FT IR (ATR, υ_{max}/cm): 33412 (-OH), 1709 (C=O of ester), 1209 (C-O of ester), 835 (C-Cl); ^{1}H NMR (400 MHz, DMSO-d_6): δ = 1.008-1.05 (t, 3H, *J* = 13 Hz, 4-CH_3), 1.44-1.49 (m, 5H, ester CH_3 and 3-CH_3), 1.94-1.98 (quint, 2H, 2-CH_2), 4.42-4.47 (q, 4H, *J* = 8 Hz, ester CH_2 and 1-CH_2), 7.12-7.14 (dd, 2H, H_3 and H_4 of 5-chloro-2-hydroxyphenyl), 7.33-7.37 (m, 1H, H_7 of benzimidazole), 7.45-7.47 (d, 1H, *J* = 8 Hz, H_8 of benzimidazole), 8.08-8.084 (dd, 1H, *J* = 1.6 Hz, H_5 of benzimidazole), 8.574-8.576 (d, 1H, *J* = 0.8 Hz, H_6 of 5-chloro-2-hydroxyphenyl) ppm; ^{13}C NMR (100 MHz): δ = 13.9, 14.1, 20.1, 30.1, 49.6, 61.2, 110.2, 110.8, 115.7, 118.3, 128.7, 129.1, 130.3, 130.5, 130.6, 134.3, 141.0, 150.8, 158.7, 167.2 ppm; MS: calculated for $C_{20}H_{21}N_2ClO_3$ is 372.12; found $[M+H]^+$ 373.05 *m/z*; Anal.calc. for $C_{20}H_{21}N_2ClO_3$: C, 64.43; H, 5.68; N, 7.51%. Found: C, 64.0; H, 5.45; N, 7.25%; Uv-Vis: λ_{max} (ACN) = 332 nm, Fluorescence: λ_{ex} = 332 nm, λ_{em} (ACN) = 486 nm, Φ = 0.30.

Ethyl 2-(5-bromo-2-hydroxyphenyl)-1-butyl-1H-benzo[d]imidazole-5-carboxylate (3d)

Off white solid; yield: 93%; melting point (°C): 128-130; FT IR (ATR, υ_{max}/cm): 3465 (-OH), 1705 (C=O of ester), 1210 (C-O of ester), 650 (C-Br); ^{1}H NMR (400 MHz, DMSO-d_6): δ =

1.007-1.04 (t, 3H, *J* = 13 Hz, 4-CH_3), 1.42-1.47 (m, 5H, ester CH_3 and 3-CH_2), 1.95-1.99 (quint, 2H, 2-CH_2), 4.40-4.45 (q, 4H, *J* = 8 Hz, ester CH_2 and 1–CH_2), 7.13-7.15 (dd, 2H, H_3 and H_4 of 5-bromo-2-hydroxy phenyl), 7.31-7.34 (m, 1H, H_7 of benzimidazole), 7.44-7.46 (d, 1H, *J* = 8 Hz, H_8 of benzimidazole), 8.06-8.09 (dd, 1H, *J* = 1.6 Hz, H_5 of benzimidazole), 8.336-8.338 (d, 1H, *J* = 0.8 Hz, H_6 of 5-bromo-2-hydroxy phenyl) ppm; ^{13}C NMR (100 MHz): δ = 13.7, 14.2, 20.4, 30.1, 49.4, 61.0, 110.2, 110.9, 116.7, 118.2, 120.1, 129.1, 130.2, 130.7, 133.3, 134.3, 141.5, 151.9, 159.5, 168.2 ppm; MS: calculated for $C_{20}H_{21}N_2BrO_3$ is 416.07; found $[M+H]^+$ 417.15 *m/z*; Anal.calc. for $C_{20}H_{21}N_2BrO_3$: C, 57.56; H, 5.07; N, 6.71%. Found: C, 57.45; H, 5.05; N, 6.65%; Uv-Vis: λ_{max} (ACN) = 332 nm, Fluorescence: λ_{ex} = 332 nm, λ_{em} (ACN) = 497 nm, Φ = 0.16.

Ethyl 1-butyl-2-(3,5-dichloro-2-hydroxyphenyl)-1H-benzo[d]imidazole-5-carboxylate (3e)

Off white solid; yield: 92%; melting point (°C): 120-122; FT IR (ATR, υ_{max}/cm): 3390 (-OH), 1707 (C=O of ester), 1219 (C-O of ester), 831, 748 (C-Cl); ^{1}H NMR (400 MHz, DMSO-d_6): δ = 1.03-1.06 (t, 3H , *J* = 12 Hz, 4-CH_3), 1.42-1.51 (m, 5H, ester CH_3 and 3-CH_2), 1.93-2.0 (quint, 2H, 2-CH_2), 4.40-4.46 (q, 4H, *J* = 8 Hz, ester CH_2 and 1-CH_2), 7.43-7.47 (m, 2H, H_4 of 3,5-dichloro-2-hydroxyphenyl and H_7 of benzimidazole), 7.536-7.542 (d, 1H, *J* = 2.4 Hz, H_4 of benzimidazole), 8.08-8.10 (dd, 1H, *J* = 1.6 Hz, 10 Hz, H_6 of benzimidazole), 8.427-8.30 (d, 1H, *J* = 1.2 Hz, H_6 of 3,5-dichloro-2-hydroxyphenyl) ppm; ^{13}C NMR (100 MHz): δ = 13.7, 14.6, 20.2, 31.9, 46.1, 61.3, 109.9, 114.7, 121.4, 123.4, 124.4, 124.7, 125.7, 126.4, 131.8, 138.2, 139.4, 151.0, 154.2, 166.7 ppm; MS: calculated for $C_{20}H_{20}N_2Cl_2O_3$ is 406.09; found $[M+H]^+$ 407.05, $[M+H+2]^+$ 409.05, $[M+H+4]^+$ 411.05 *m/z*; Anal.calc. for $C_{20}H_{20}N_2Cl_2O_3$: C, 58.98; H, 4.95; N, 6.88%. Found: C, 58.95; H, 4.90; N, 6.70%; Uv-Vis: λ_{max} (ACN) = 336 nm, Fluorescence: λ_{ex} = 336 nm, λ_{em} (ACN) = 500 nm, Φ = 0.87.

Characterization details

The determination of the melting point was done by an open capillary method and was uncorrected. Bruker Avance III, 400 MHz was used to record ^{1}H NMR and ^{13}C NMR spectra. The chemical shift values were stated in parts per million (ppm) and coupling constants in Hertz (Hz). TMS was used as an internal standard. FT (ATR)-IR absorption spectra were recorded on Shimadzu, in the range 4000–400 cm^{-1}. Mass spectra were recorded on Schimadzu LCMS-8030 and are uncorrected. Thin layer chromatography on a silica-coated aluminium sheet was used to check the completion of the reaction and for checking the purity. Ethylacetate and hexane (3:7, v/v) were used as mobile phase. The UV-vis spectra of the derivatives were

measured in ACN, EtOH, DMF, DMSO and THF solvents (concentration 2.66 x 10^{-5} M and 2 x 10^{-6} M) at room temperature using Shimandzu spectrometer. The photoluminescence (PL) spectra were recorded in Hitachi, Japan F-7000 Fluorescence Spectrophotometer. The florescence quantum yield was calculated using equation 1.

$$\Phi = \Phi_R \frac{I}{I_R} \frac{OD_R}{OD} \frac{n^2}{n_R^2} \quad (1)$$

Where I is the integrated intensity, OD is the optical density and n is the refractive index, the subscript R refers to the reference fluorophore of known quantum yield [29]. The fluorescence lifetimes were measured employing picosecond time domain spectrometer based on Time Correlated Single Photon Counting (TCSPC) technique (IBH Jobin Yvon 6.1). All the samples were excited at around 330 nm in ACN solvent using pulsed excitation source (NanoLED) in an IBH Fluorocube apparatus. apparatus. The fluorescence emission was counted by a Hamamatsu Micro Channel Plate Photo-multiplier tube (R3809 MCP-PMT). The thermogravimetric analysis (TGA) was carried out to determine the thermal stability using STA-2500, NETZSCH, Germeny at a heating rate of 10 °C min^{-1} under an inert atmosphere. The cyclic voltammetry (CV) was carried out by using three-electrode system. The experiment was conducted in Ivium vertex electrochemical work station with 100 mV s^{-1} scan rate, in which platinum wire used as a counter electrode, working electrode used was material coated glassy carbon electrode and saturated calomel electrode (SCE) as a reference electrode. The supporting electrode used was tetrabutylammoniumhexafluorophosphate (0.1 M) in acetonitrile solvent. The measurements were calibrated using ferrocene/ferrocenium (Fc/Fc^+) standard. The density functional theory (DFT) and molecular electrostatic potential (MEP) were carried out using Acer Veriton i5 Workstation using Materials Science Suite 2017-1, Schrödinger LLC, New York, NY, 2017. The X-ray intensity data for compounds **3a** and **3e** were collected at a temperature of 293 K on a Rigaku Saturn724 diffractometer using graphite monochromated Mo-Kα radiation. A complete data set was processed using *CrystalClear* [30]. The structures were solved by *SHELXS* and *SHELXL* programs [31]. The geometrical calculations were carried out using the program *PLATON* [32]. The molecular and packing diagrams were generated using software *MERCURY* [33].

RESULTS AND DISCUSSIONS

Synthesis and Characterization

The synthetic route for compounds **3a-e** is depicted in the **Scheme 1** given below. The synthesis of the target compound was obtained in three simple steps according to the reported procedure [34]. Firstly, 4-chloro-3-nitrobenzoic acid in ethanol was refluxed in the presence of catalytic amount conc. H_2SO_4 to afford ethyl 4-chloro-3-nitrobenzoate (**1**). Intermediate **1** undergoes nucleophilic substitution reaction upon treatment with n-butylamine in the presence of triethylamine as a base in dry THF at room temperature to give ethyl 4-(butylamino)-3-nitrobenzoate (**2**). Intermediate **2** on treatment with substituted salicylaldehyde in the presence of sodium dithionite as a reducing agent in DMSO undergoes one-pot nitro reductive cyclisation to yield the title compounds **3a-e**. The obtained products were purified by recrystallisation in DMF. All these compounds can be stored for a longer time under the ambient conditions without any detectable degradation. The formation of the products was confirmed by ^{1}H NMR, ^{13}C NMR, MS, FTIR, single crystal XRD and elemental analyses.

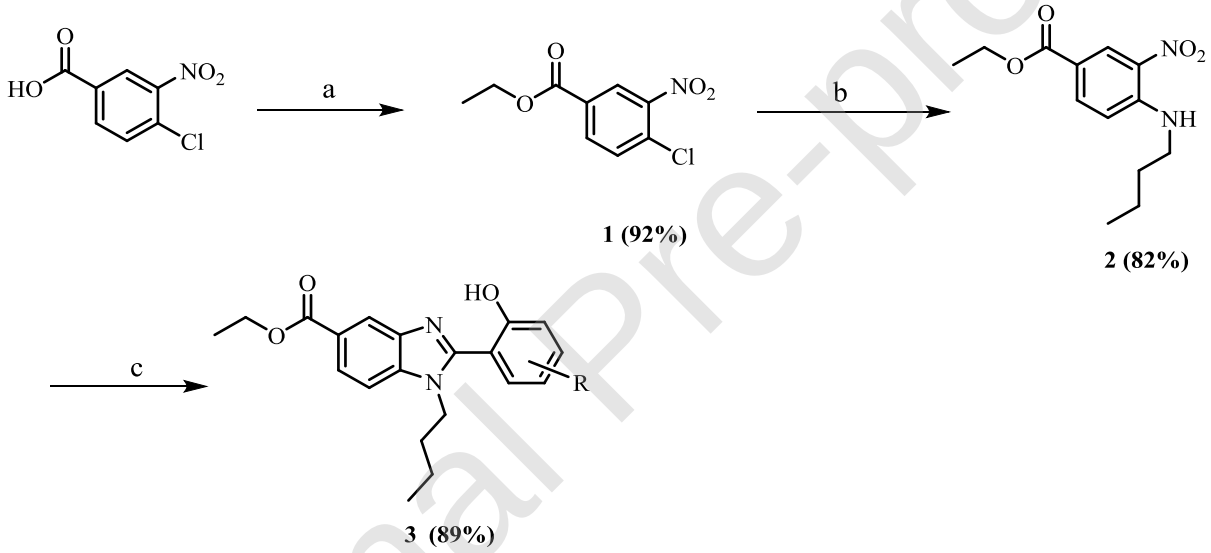

3a: R = H, **3b**: R = 5-F, **3c**: R = 5-Cl, **3d**: R = 5-Br, **3e**: R = 3,5-Cl_2

Scheme 1: The synthesis of target compounds (**3a-e)**. Reagents and conditions: (a) H_2SO_4, dry ethanol, 16 h; (b) n-Butylamine, triethylamine, room temperature; (c) substituted salicaldehydes, sodium dithionite, 90 °C, 3 h.

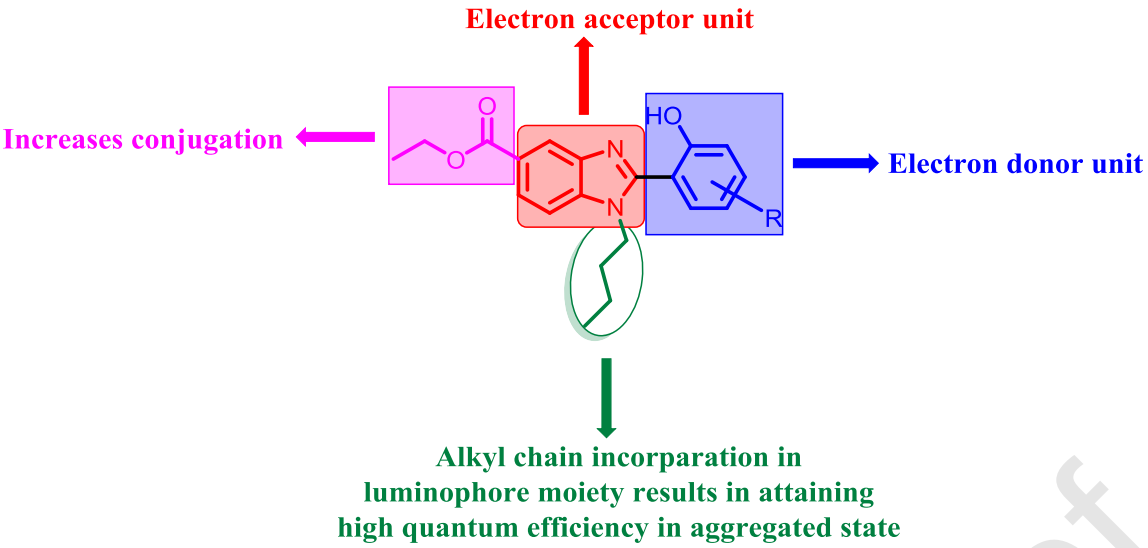

Fig. 2: Synthetic strategy for designing target molecule

Formation of **3b** to the consideration, ^{1}H NMR spectrum showed triplet at 1.00-1.04, multiplet at 1.42-1.47, quintet at 1.95-1.99 and quartet at 4.40-4.45 ppm confirmed the presence of *N*-butyl and ethyl ester group. The signal doublet of doublet at 7.10-7.12 ppm with J = 4 Hz, 1.6 Hz was attributed for H_3 and H_4 of 5-fluoro-2-hydroxy phenyl due to *meta* and *para* coupling. Whereas multiplet at 7.32-7.35 ppm was attributed for H_7 of benzimidazole, H_8 of benzimidazole showed a doublet with J = 8 Hz at 7.43-7.45 ppm due to *ortho* coupling. Furthermore, signals in the region 8.06-8.09 and 8.472-8.474 were assigned for H_5 of benzimidazole with J = 1.6 Hz represented meta coupling and H_6 of 5-fluoro-2-hydroxy phenyl having J = 0.8 Hz showed *para* coupling respectively. The formation of the product was supported by ^{13}C NMR spectrum with a characteristic peak at 166.9 ppm for carbonyl carbon of ester and 154.3 ppm for carbon attached to hydroxy group.

Crystal structures and Thermal Properties

The crystals suitable for X-ray analysis of **3a** and **3e** were obtained using slow evaporation method. The molecular and crystal structure of **3a** and **3e** confirmed using X-ray crystallographic studies (**Fig. 3. and Fig. 5.**). In the title compounds **3a** and **3e**, (**Fig. 4, Fig. 6** and **Table 1**), the molecules are connected through C11---H11A…O2 and C17---H17B…O2 intermolecular hydrogen bonds. The intramolecular hydrogen bonds of the type O3---H3…N2 are observed in both the compounds. The Cg…Cg short interactions in molecule **3a** are, Cg1…Cg1 (3.747 (2) **Å**, slippage = 1.281 **Å**, -X,-Y,-Z), Cg1…Cg3 (3.6532 **Å**), -X,1-Y,-Z) and Cg2…Cg3 (3.696(2) **Å**, -X,-Y,-Z). Where, Cg1: N1/C7/N2/C6/C8, Cg2:C4-C10 and Cg3:

C15-C20. The molecule **3e** has short interactions of the type Cg2…Cg2 (3.712(2) **Å**, 1-X,-Y,1-Z, slippage = 0.722), Cg2…Cg4 (3.683(2) **Å**, -X,-Y,1-Z) and Cg3…Cg4 (3.767(2) **Å**, 1-X,-Y,1-Z). Where, Cg2: N1/C7/N2/C6/C8, Cg3: C4-C10and Cg4: C11-C16. The bond length and bond angles of **3a** and **3e** are included in ESI (**Table S4-S9**).

Thermogravimetric analysis (TGA) was carried out to determine the thermal stability of the molecules (**3a-e**). The TGA plots are shown in **Fig. S15** (ESI). The compounds **3a**, **3b**, **3c**, **3d** and **3e** show high decomposition temperature (T_d) of 259, 221, 252, 270 and 266 °C, respectively and 5%, 19%, 34%, 2% and 17 % of compounds **3a-e** left as residual matter. Among five synthesized compounds (**3a-e**), **3d** showed the highest decomposition temperature. Whereas, the amount of compound left as the residual matter is highest for **3c** indicating highest stability among the five synthesized compounds (**3a-e**) (**Table 2**).

Table 1: Intramolecular and Intermolecular interactions parameters

D---H... A/Cg	**D---H (Å)**	**H...A/Cg/X (Å)**	**D....A/CgX (Å)**	**D---H... A/Cg/X (°)**	**Symmetry**
3a					
O3---H3…N2	0.82	1.79	2.524(5)	149	
C11---H11A…O2	0.97	2.56	3.493(6)	161	x,1/2+y,1/2-z
3e					
O3---H3…N2	0.82	1.80	2.524(5)	146	
C17---H17B…O2	0.97	2.51	3.422(9)	156	1-x,-y,1-z

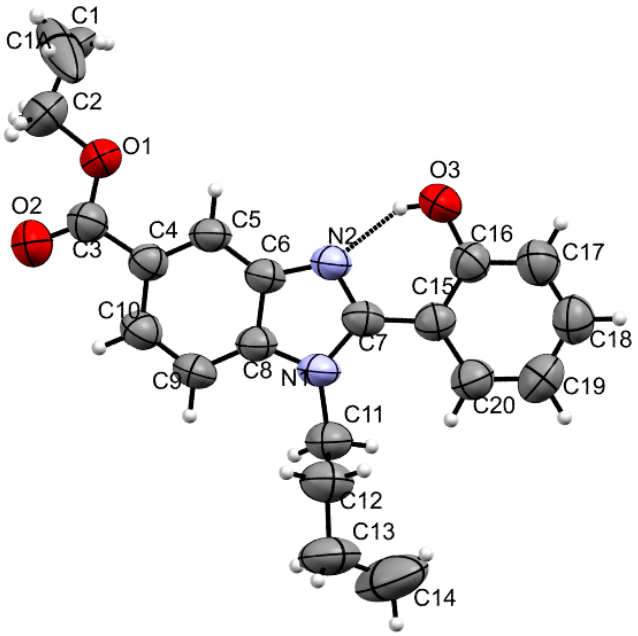

Fig. 3: ORTEP diagram of Ethyl 1-butyl-2-(2-hydroxyphenyl)-1*H*-benzo[*d*]imidazole-5-carboxylate (**3a**)

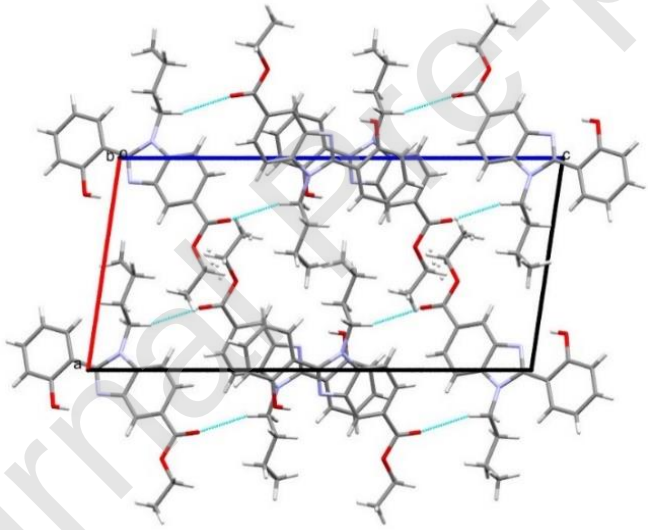

Fig. 4: Packing of the **3a** molecules when viewed down along the *b*-axis. The dotted lines represent intermolecular hydrogen bonds.

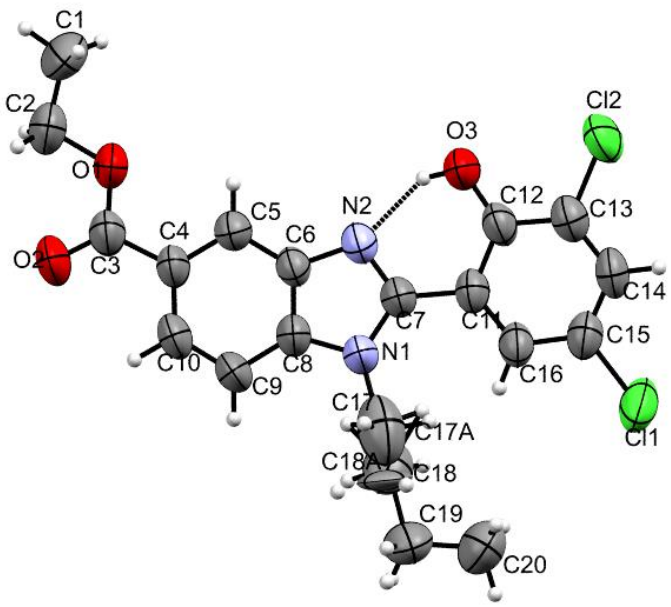

Fig. 5: ORTEP diagram of Ethyl 1-butyl-2-(3,5-dichloro-2-hydroxyphenyl)-1*H*-benzo[*d*]imidazole-5-carboxylate (**3e**)

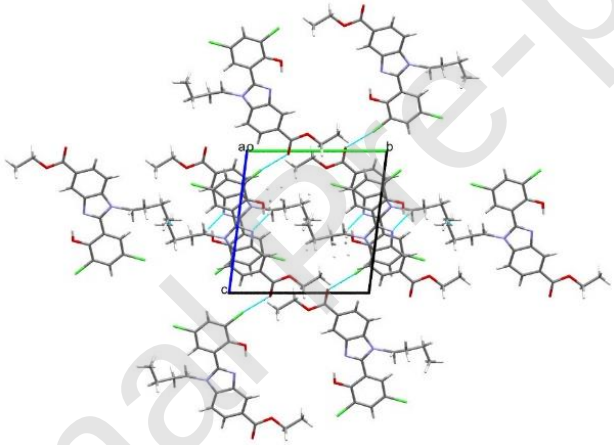

Fig. 6: Packing of the **3e** molecules when viewed down along the *b*-axis. The dotted lines represent intermolecular hydrogen bonds.

Photophysical Properties

UV-vis studies Photoluminescence (PL) spectral studies

The photophysical properties of the benzimidazole derivatives were measured using UV-vis absorption and photoluminescence (PL) spectroscopy**.** The UV-vis absorption of the synthesized compounds (**3a-e**) was studied at room temperature. **Fig. 7** shows UV-vis absorption spectra of **3a-e** in acetonitrile. The synthesized benzimidazole derivatives have a hydroxy-substituted aromatic ring with continuous conjugation with a benzimidazole-5-carboxylate moiety which shows two main groups of bands in absorption spectra observed at

220-290 nm and 330-335 nm. The strong absorption band at a shorter wavelength is due to the π-π* of the hydroxy-substituted aromatic ring towards benzimidazole moiety [35]. The relatively weak absorption band at higher wavelength is due to π-π* transition within the whole molecule. The maximum absorption wavelengths ($\lambda_{\max}^{abs}$) of **3a**, **3b**, **3c**, **3d** and **3e** were observed at 322, 332, 332, 332 and 336 nm respectively.

Photoluminescence (PL) spectral studies

All chromophores exhibit dual emission bands around 500 nm (i.e., strong main band) and 369 nm (i.e., weak sub band) in weak H-bonding solvent such as acetonitrile at room temperature. This dual emission originates from phototautomerization (i.e., excited-state intramolecular proton transfer (ESIPT)) that changes enol form (E) to keto form (K) upon excitation, by migrating a proton to the neighbouring electronegative atom through intramolecular H-bonding **(see Scheme 2).** After relaxation of the K-form to the ground state, the E-form is again recovered by ground-state intramolecular proton transfer (GSIPT) i.e., reverse proton transfer [36-39]. Further, **Fig. 3 and Fig. 5** confirms that 2-hydroxyphenyl benzimidazole derivatives exhibit intramolecular hydrogen bonding of type O3---H3…N2. The weak shorter wavelength emission (369 nm) is the normal emission from excited enol whereas strong longer wavelength emission (474-500 nm) is from tautomer due to ESIPT [40, 41]. Usually the tautomer emission has highest Stokes shift [42].

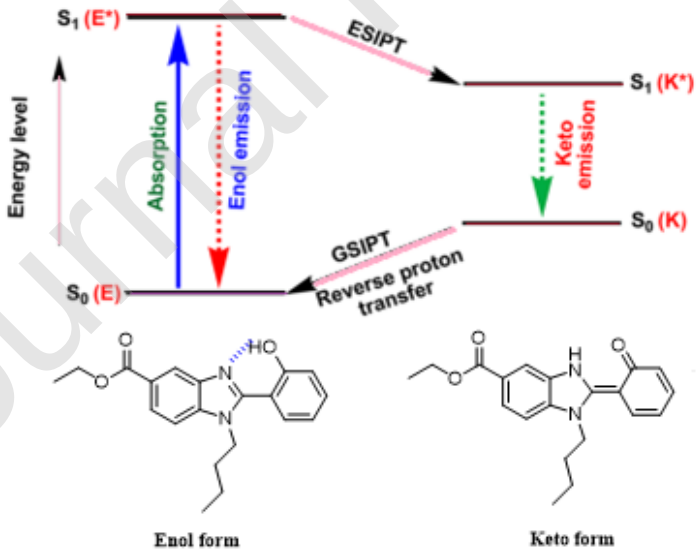

Scheme 2: Typical schematic representation of the Four Level ESIPT Photocycle for 3a compound

The tautomer emission found to be red shifted on changing the substitution on 2-hydroxyphenyl moiety. Whereas normal emission did not display any changes. The slight red shift in tautomer emission spectra of compounds **3b-e** compared to **3a** (**Fig. 7**) was due to the presence of halogen atom in the fifth position of the hydroxy phenyl moiety. It was observed that as the size of the halogen atom increases emission maxima showed bathochromic shift. The molecule **3e** with 3,5-Cl_2 substitution in the hydroxyphenyl moiety showed the highest emission maxima at 500 nm. The emission maxima of compounds **3a-e** is in the order **3e** > **3d** > **3b** > **3c** > **3a** with wavelength 500, 497, 486, 487and 474 nm respectively (**Table 2**). Even though the marginal difference was observed concerning for to emission maxima, but there was a huge difference in intensity of these compounds due to variation in the structural property. The moiety with 3,5-Cl_2 (**3e**) substituted in hydroxy phenyl showed the highest intensity compared to other moieties in the series followed by **3c**, **3d**, **3b** and **3a**.

Solid state photoluminescence studies

The emission spectra of compounds **3a-e** in solid-state films were obtained by exciting at 300 nm (**Fig. 7**) and the $\lambda_{\max}^{emi}$ being 481-509 nm which fall within blue to green region. The results revealed that there were about 9-14 nm of the bathochromic shift in a solid state when compared to the solution phase which explains the existence of aggregation induced emission. The absorption and emission maxima of compounds **3a-e** were summarised in **Table 2**.

The degree of a bathochromic shift from absorption maxima ($\lambda_{\max}^{abs}$) to emission maxima ($\lambda_{\max}^{emi}$) is measured by the Stokes shift which is the range of 151-165 nm. Among five title compounds, **3a** and **3e** showed smaller and larger stokes effect respectively (**Table 2**).

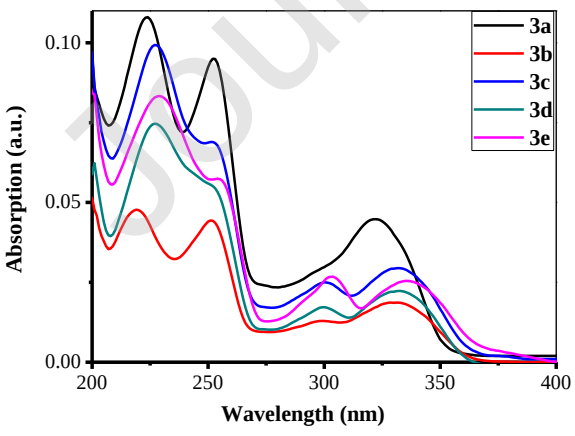

(a)

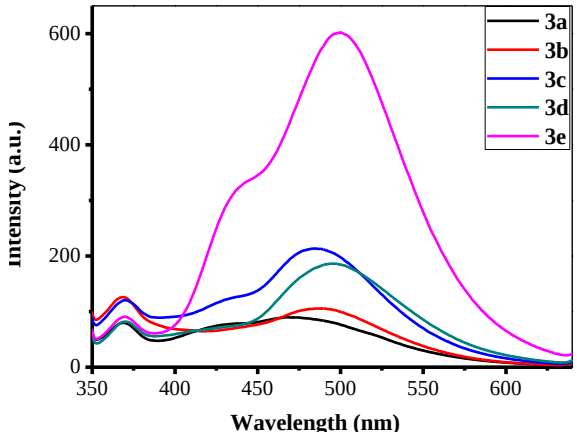

(b)

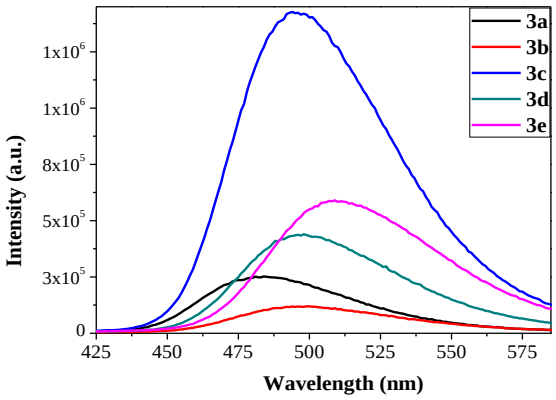

(c)

Fig. 7: (a) UV-Vis absorption spectra of compounds **3a-e** in ACN at room temperature, at 2 µM concentration

(b) Emission spectra of compounds **3a-e** in ACN at room temperature, at 2 µM concentration excited at λ_{ex} = 330 nm.

(c) Emission spectra of compounds **3(a-e)** in solid state film when excited at λ_{ex} = 300 nm.

Quantum Yield (Φ) calculations

Fluorescence quantum yield (Φ_{PL}) were measured in ACN at room temperature and compared with 2-napthylamine taken as a reference of known quantum yield (**Fig. S18**). The radiative (kr) and non-radiative rate constants were calculated using Φ_{PL} and lifetime values. It was observed that moieties with chlorine substituent showed highest quantum yield compared to other halogen atoms. The highest Φ_{PL} value of 0.87 was observed for **3e**, which is due to decrease of non-radiative rate constant based on tight packing structure with hydrogen-bonds (see **Table 2**). The comparison between previously reported benzimidazole derivatives [35, 43-46] and **3e** has been summarised in **Table S10** (ESI). The introduction of the ehtylester and alkyl chain greatly enhanced the optoelectronic property, quantum yield and Stokes shift. Alkyl group greatly affects the solid-state fluorescence behaviour of small organic luminophore [47] and introduction of ethylester which is in continuous conjugation with benzimidazole nucleus leads to an intramolecular charge transfer due to which emission peaks are redshifted depending on the nature of electron-acceptor unit [48]. (**Fig. 2**). The moderate Φ_{PL} was observed for the rest of the derivatives which was in the range of 0.03-0.3 (**Table 2**). The compound with fluorine substituent (**3b**) showed the least fluorescence quantum yield of 0.03 because of increased non-radiative rate constant.

Table 2: Summary of Optical and thermal properties of compounds (**3a-e)**

Comp.	Absorption λ_{max}^{abs} (nm)[a]	Emission			Stoke shift Δλ (nm)	Φ_{PL}	T_d[°C][e]	Average lifetime (ns)	Radiative rate constant kr ($\times 10^8 S^{-1}$)	Non-radiative rate constant knr ($\times 10^9 S^{-1}$)
		λ_{max}^{emi} (nm)[b]		λ_{max}^{emi} (nm)[c]						
		Normal emission	Tautomer emission							
3a	322	369	474	483	152	0.14	259	0.31	4.52	2.77
3b	332	369	487	500	155	0.03	221	0.26	1.15	3.73
3c	332	369	486	495	154	0.30	252	0.21	14.3	3.33
3d	332	369	497	498	156	0.16	270	0.26	6.15	3.23
3e	336	369	500	510	165	0.87	266	1.21	7.19	0.11
Std[d]	345	369	400	-	55	0.91	-	-	-	-

[a]The absorption spectra were measured in acetonitrile at 2 x 10^{-6} M concentration.

[b]The emission spectra were measured in acetonitrile at 2 x 10^{-6} M concentration.

[c]The emission spectra were measured in solid state film.

[d] 2-Napthylamine was used as a standard compound.

[e]Obtained TGA measurements.

Solvent Effect

The role of solvent is important in spectroscopic analysis as it brings major changes in intensity, shape and position of absorbance and fluorescence band. Hence to study the solvent-induced shift in absorption and emission band and to understand the intramolecular charge transfer (ICT) effect, the UV-vis and photoluminescence study of molecules **3a-e** were studied in solvents of different dielectric constant with a set concentration of 2.66 x 10^{-5} M. The chosen solvents are tetrahydrofuran (THF), *N*,*N*-dimethylformamide (DMF), ethanol (EtOH) and dimethyl sulfoxide (DMSO). The results are summarised in **Table S11** and depicted in **Figs. S10-14** (ESI). The spectral shifts with respect to solvent polarity reflects on the molecular interactions between solute and solvent. The spectral curves revealed that molecules **3a-e** displayed an absorption peak in the region 274-337 nm. Finite bathochromic shifts were observed differing by 2-25 nm on varying substitution on hydroxyphenyl moiety. Further, it was observed that on increasing the solvent polarity absorbance maxima shifted to blue region. A similar trend in absorption maxima of compounds **3a-e** on varying solvent polarity was

observed that is, EtOH < DMF = DMSO < THF. About 25-51 nm of a shift to blue region was observed on increasing solvent polarity.

The solution photoluminescence (PL) spectra of all the derivatives showed an emission band in the violet-green region (352-508 nm). The compound **3a**, **3b** and **3c** exhibited dual emission in THF solvent, whereas single emission in EtOH, DMF and DMSO solvent which is attributed to intramolecular hydrogen bonding dominates over solvent-solute interaction in THF solvent resulting in dual emission. Whereas compound **3d** and **3e** displayed dual emission in all chosen solvents. The absence of dual emission in few solvents suggests the absence of ESIPT process due to the presence of intermolecular hydrogen bonding with solvent molecule resulting in the stabilization of solvated isomer [36] (**Fig. S19**, ESI). Usually the tautomer emission has highest Stokes shift. Hence it can be inferred that single emission at longer wavelength is tautomer emission. Also, photoluminescence spectra were intense in the EtOH solvent which indicates the stabilization of the dipole moment of the molecules in the excited state by the solvent. Among the series **3a-e**, compound **3e** showed the highest Stokes shift in EtOH solvent. Furthermore, it was observed that on increasing the solvent polarity emission maxima shifted to red region.

Fluorescence lifetime studies

The fluorescence decay of **3a-e** was measured in ACN solvent (**Fig. S20** in ESI) and the data were tabulated in **Table 2**. When excited around 330 nm, dual lifetimes were noticed for all compounds (see **Table S13** in ESI). The biexponential decay was perhaps due to dual emission bands. The shorter lifetime values (i.e., $\tau 1$) corresponds to the excited E-form and the longer lifetime values (i.e., $\tau 2$) corresponds to K-form of **3a-e** compounds. The excited state lifetimes vary from 0.21 ns (least for **3c**) to 1.21 ns (highest for **3e**).

Electrochemical Properties

To explore electrochemical properties and practical energy levels of the molecules (**3a-e**), cyclic voltammetry studies were performed (**Table S12, ESI**). The cyclic voltammograms of molecules (**3a-e**) is depicted in **Fig. S16 (ESI)**. The molecules **3a-e** exhibited one oxidation potential peak in the anodic region at 0.99, 0.92, 0.99, 0.96, 1.00 V vs SCE respectively. The highest occupied molecular orbital (HOMO) was calculated using equation (2)

$$E_{HOMO} = -[E^{ox}_{onset} + 4.8eV - E_{FOC}] \quad (2)$$

where, E_{onset}^{ox} and E_{FOC} are the onset oxidation potentials of the compounds and ferrocene (E_{FOC} = 0.29 V vs SCE (**Fig. S17, ESI**)), respectively, −4.8 eV is the HOMO energy level of ferrocene against vacuum.

Whereas, lowest unoccupied molecular orbital (LUMO) energy levels were calculated using equation (3).

$$E_{LUMO} = E_{HOMO} + E_g \quad (3)$$

The optical bandgap value (E_g) estimated from the absorption edge of **3a-e** were 3.51, 3.42, 3.42, 3.41, 3.37 respectively, calculated using equation (4) which varied in the order **3a** > **3b** = **3c** = **3d** > **3e**.

$$Eg = \frac{1240}{\lambda onset} \quad (4)$$

The calculated HOMO-LUMO energy gap of **3a-e** using equation (5) are summarised in **Table S12**. The results revealed that there was a marginal difference of HOMO-LUMO energy gap of benzimidazole ligands.

$$\Delta E = E_{HOMO} - E_{LUMO} \quad (5)$$

DFT calculation and electronic structures

The quantum parameters like highest occupied molecular orbital (HOMO), lowest unoccupied molecular orbital (LUMO) and HOMO-LUMO bandgap are essential to determine the chemical stability as well as molecular electrical transport properties of the synthesized molecule [49]. To obtain the knowledge about the electronic structure of newly synthesized benzimidazole derivatives, theoretical computational studies were carried out by density function theory (DFT) with basis set ps-321G, ps-631G and ps-6311G for compounds **3a**, **3b**, **3c** and **3e**. Whereas ps-LAV3P basis set for compound **3d**. The optimized structure, HOMO and LUMO distribution of **3a-e** is depicted in **Fig. 8**. The HOMO of the title compounds is localized on the whole conjugated molecular backbone excluding the ester group and n-butyl group. Whereas, LUMO is localized on the whole conjugated molecular backbone as well as on ester moiety but excluding n-butyl group. The calculated energies of HOMO are in the range of -6.15 to -6.49 eV whereas LUMO in the range of -1.62 to -2.00 eV. The incorporation of two chlorine atom in **3e** effectively lowered the LUMO energy level which leads to the bathochromic shift in electronic absorption. DFT-based reactive descriptors resulted from HOMO-LUMO energies are summarized in **Table S12 (ESI)**.

The perception of electronegativity (χ), global hardness (η), global softness (S) and electrophilicity index (ω) can be calculated [50] according to Koopman's theorem using HOMO and LUMO energies (**Table 3**). The chemical behaviour of the synthesized compound can be predicted by these parameters. The moiety is defined as acidic with higher χ value. Whereas, the moiety is considered as basic with smaller χ value. The acidic character of the synthesized molecule follows the order **3c** > **3b** > **3a** > **3d** > **3e**. The stability of the molecule is determined by the global hardness which is the order **3e** > **3c** > **3a** > **3b** > **3d**. Whereas global softness in the order **3d** > **3a** = **3b** = **3c** > **3e** indicating **3d** is soft and more reactive compared to other moieties. The electrophilicity index values are in the order **3c** > **3b** > **3a** > **3d** > **3e** indicating all are highly electrophilic.

COMPOUNDS	OPTIMISED GEOMETRY	HOMO	LUMO
3a	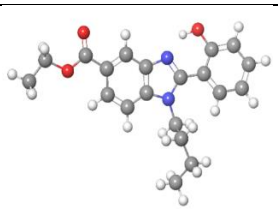	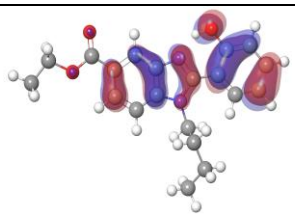	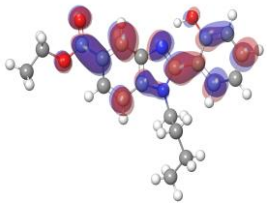
3b	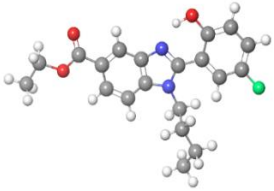	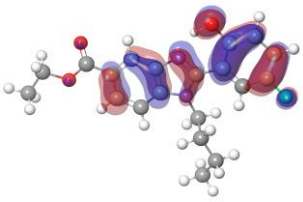	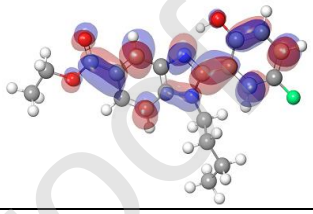
3c	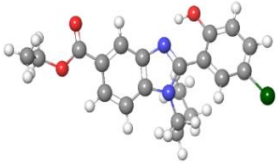	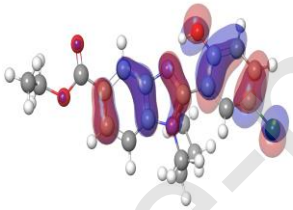	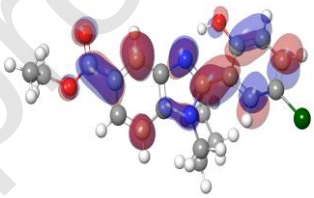
3d	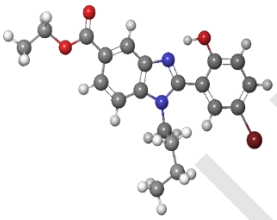	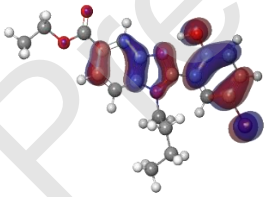	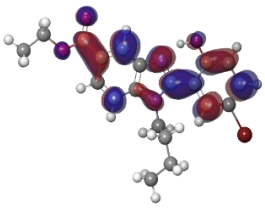
3e	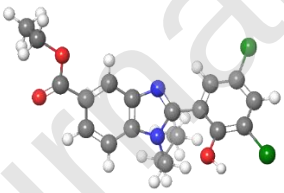	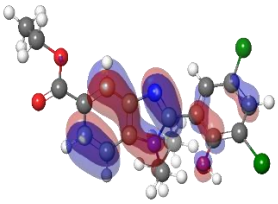	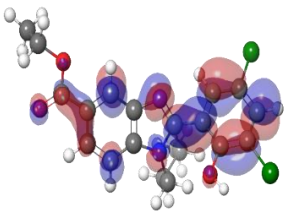

Fig. 8: Calculated molecular orbital plots of HOMO and LUMO levels and optimized molecular structures of compounds **3a-e**.

Table 3: Conceptual DFT-based reactivity descriptors for the synthesized compounds **3a-e**

Parameter	**3a**	**3b**	**3c**	**3d**	**3e**	Derivation
Ionization potential (*I*) (eV)	6.34	6.40	6.50	6.15	6.23	$I = -E_{HOMO}$
Electron affinity (*A*) (eV)	2.00	2.12	2.15	1.90	1.63	$A = -E_{LUMO}$
Chemical potential (μ) (eV)	-4.17	-4.26	-4.32	-4.03	-3.93	$\mu = -(I + A)/2$
Electronegativity (χ) (eV)	4.17	4.26	4.32	4.03	3.93	$\chi = -\mu$
Global hardness (η) (eV)	4.34	4.28	4.35	4.25	4.60	$\eta = I - A$
Global softness (*S*) (eV^{-1})	0.23	0.23	0.23	0.24	0.22	$S = 1/\eta$
Electrophilicity index (ω) (eV)	2.00	2.12	2.14	1.91	1.68	$\omega = \mu^2/2\eta$

Molecular Electrostatic Potential (MEP)

MEP surface reveals the dispersal of charges across the surface of a molecule and it is a very useful tool for understanding hydrogen bonding interactions, nucleophilic and electrophilic sites of the synthsized molecule [51]. The prediction of reactive sites of the compounds **3a-e** was obtained using the ps-321G, ps-631G and ps-6311G basis sets for compounds **3a**, **3b**, **3c** and **3e**. Whereas ps-LAV3P basis set for compound **3d** which are shown in **Fig. 9**. The colours represent the magnitude of electrostatic potential. Blue colour represents the strongest attraction; electron-deficient region while red colour represents the strongest repulsion; electron-rich region. In contrast, red regions are prone to electrophilic attack while blue regions to nucleophilic attack. These results give us evidence about which region of the molecule undergoes intermolecular interaction when the reaction is carried out. From MEP surface it is evident that the red region is localised on the N_3 of benzimidazole, oxygen atom of ester, fluorine atom and hydroxy group while the blue region is localised on the carbonyl carbon, hydrogen atoms of the aromatic region and the hydrogen atom of the hydroxy group. The dark blue colour region indicates the high reactivity towards nucleophiles while light blue regions are less reactive.

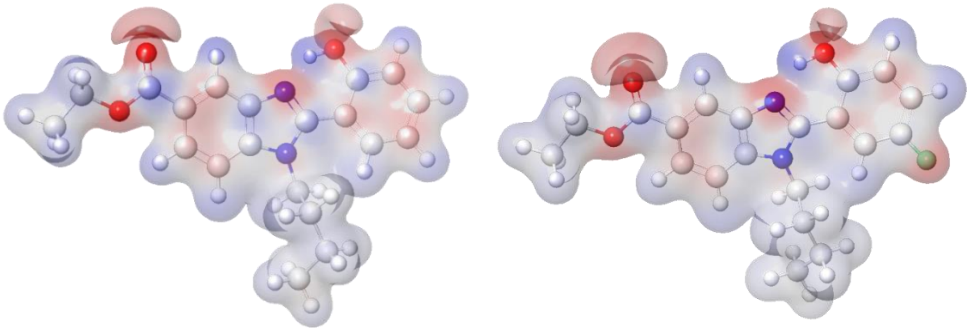

3a **3b**

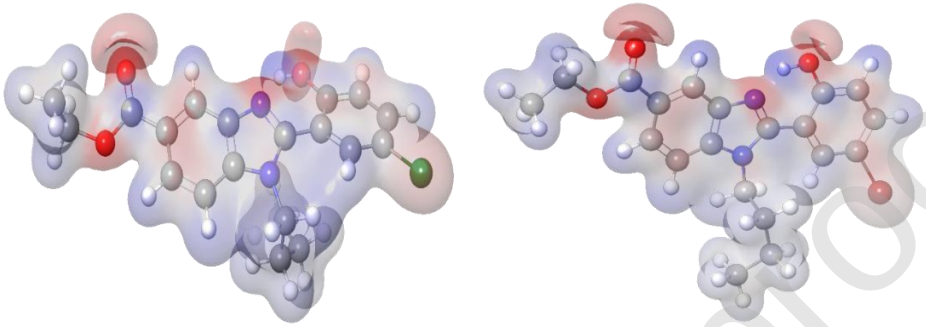

3c **3d**

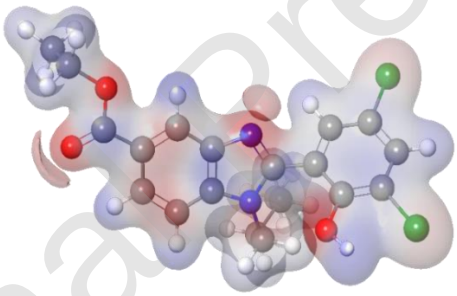

3e

Fig. 9: Molecular Electrostatic Potential (MEP) of compounds **3a-e**

Conclusions

Five novel benzimidazole derivatives have been synthesized *via* "one-pot" nitro reductive cyclization using one of the cheaply available reagent sodium dithionite. The three-dimensional crystal structures of **3a** and **3e** were confirmed using single-crystal X-ray diffraction method. The introduction of halogen atoms to 2-hydroxyphenyl group attached to benzimidazole moiety resulted in a bathochromic shift in UV-Vis and PL spectra, as well as resulted in increased molecular stability. These moieties also exhibit blue-green fluoresce in solid-state. The HOMO-LUMO bandgap energy obtained from DFT and CV are fairly in agreement. The

fluorescence quantum yield was found to be appreciable for benzimidazole derivative compared to reference (2-Napthylamine). Especially compound **3e** showed green emission, dual emission in both polar protic and aprotic solvents, high quantum yield, highest excited state lifetime and good thermal stability. The findings of results help in developing novel ligand in the field of organic optoelectronics.

Supporting information

Supporting information includes spectral characterization of compounds **3a-e**, TGA graph solvent-dependant, cyclic voltammetry graphs and tables. Also, bond length and bond angle tables of **3a** and **3e**.

Declaration of interests

The authors declare that they have no known competing financial interests or personal relationships that could have appeared to influence the work reported in this paper.

Acknowledgement

Authors are thankful to Nithin Pathoor, IIT Bombay for helping in conducting solid state fluorescence; B. Ramachandra Bhat, NITK Surathkal for providing lab facility for carrying out cyclic voltammetry; DST-PURSE Laboratory, Mangalore University and CeNS Bangalore for analytical data; USIC, Karnataka University Dharwad for fluorescence lifetime and Department of Biochemistry, Mangalore University for computational studies. MKS thank IOE and DST PURSE, Vijnana Bhavan, University of Mysore, Mysuru.

References

1. N. T. Kalyani, S. J. Dhoble, Organic light emitting diodes: Energy saving lighting technology—A review, Renew Sust. Energ. Rev. 16 (2012) 2696-2723.

2. V. C. Bender, T. B. Marchesan, J. M. Alonso, Solid-state lighting: A concise review of the state of the art on LED and OLED modelling, IEEE Ind. Electron. Mag. 9 (2015) 6-16.

3. A. P. Kulkarni, C. J. Tonzola, A. Babel, S. A. Jenekhe, Electron transport materials for organic light-emitting diodes, Chem. Mater. 16 (2004) 4556-4573.

4. M. Kasha, Perturbation of the tautomerization potential, J. Chem. Soc. Faraday Trans. 2, 82 (1986) 2379-2392.

5. J. E. Kwon, S.Y. Park, Advanced organic optoelectronic materials: Harnessing excited-state intramolecular proton transfer (ESIPT) process. Adv. Mater. 23 (2011) 3615-3642.

6. D. B. O'Connor, G. W. Scott, D. R Coulter, A. Yavrouian, Temperature dependence of electronic energy transfer and quenching in copolymer films of styrene and 2-(2'-hydroxy-5'-vinylphenyl)-2H-benzotriazole, J. Phys. Chem. 95 (1991) 3615-3642.

7. S. Santra, S. K. Dogra, Spectral characteristics of 2-(2′-aminophenyl) benzimidazole in β-cyclodextrin. J. Photochem. Photobiol. A. 101 (1996) 221-227.

8. P. T. Chou, M. L. Martinez, J. H. Clements, Reversal of excitation behavior of proton-transfer vs. charge-transfer by dielectric perturbation of electronic manifolds. J. Phys. Chem. 97 (1993) 2618-2622.

9. S. Park, O.H. Kwon, Y.S. Lee, D.J. Jang, S.Y. Park, Imidazole-Based Excited-State Intramolecular Proton-Transfer (ESIPT) Materials: Observation of Thermally Activated Delayed Fluorescence (TDF), J. Phys. Chem. A 111 (2007) 9649–9653.

10. R. H. Friend, R. W. Gymer, A. B. Holmes, J. H. Burroughes, R. N. Marks, C. D. D. C. Taliani, D. D. C. Bradley, D. A. Dos Santos, J. L. Bredas, M. Logdlund, W. R. Salaneck, Electroluminescence in conjugated polymers, Nature. 397 (1999) 121-128.

11. J. Luo, Z. Xie, J. W. Lam, L. Cheng, H. Chen, C. Qiu, H. S. Kwok, X. Zhan, Y. Liu, D. Zhu, B. Z. Tang, Aggregation-induced emission of 1-methyl-1, 2, 3, 4, 5-pentaphenylsilole, ChemComm. 18 (2001) 1740-1741.

12. J. Huang, N. Sun, Y. Dong, R. Tang, P. Lu, P. Cai, Q. Li, D. Ma, J. Qin, Z. Li, Similar or totally different: the control of conjugation degree through minor structural modifications, and deep- blue aggregation- induced emission luminogens for non- doped OLEDs, Adv. Funct. 23 (2013) 2329-2337.

13. W. Z. Yuan, P. Lu, S. Chen, J. W. Lam, Z. Wang, Y. Liu, H. S. Kwok, Y. Ma, B. Z. Tang, Changing the behavior of chromophores from aggregation- caused quenching to aggregation-

induced emission: development of highly efficient light emitters in the solid state, Adv. Mater. 22 (2010) 2159-2163.

14. I. Celik, G. Ayhan-Kilcigil, B. Guven, Z. Kara, A. S. Gurkan-Alp, A. Karayel, A. Onay-Besikci, Design, synthesis and docking studies of benzimidazole derivatives as potential EGFR inhibitors, Eur. J. Med. Chem. 173 (2019) 240-249.

15. K. Deepak, P. Arora, Review on: Benzimidazole derivatives as potent biological agent, Curr. Pharm. Res. 9 (2018) 2676-2694.

16. H. Bektas, C. Albay, B. B. Sokmen, S. Aydin, E. Menteşe, G. Aydin, D. Şen, Synthesis, Antioxidant, and Antibacterial Activities of Some New 2- (3- fluorobenzyl)- 1H-benzimidazole Derivatives, J. Heterocycl. Chem. 55 (2018) 2400-2407.

17. N. T. Gowda, C. V. Kavitha, K. K. Chiruvella, O. Joy, K. S. Rangappa, S. C. Raghavan, Synthesis and biological evaluation of novel 1-(4-methoxyphenethyl)-1H-benzimidazole-5-carboxylic acid derivatives and their precursors as antileukemic agents, Bioorg. Med. Chem. lett. 19 (2009) 4594-4600.

18. H. J. Kwak, Y. M. Pyun, J. Y. Kim, H. S. Pagire, K. Y. Kim, K. R. Kim, S. Dal Rhee, W. H. Jung, J. S. Song, M. A. Bae, D. H. Lee, Synthesis and biological evaluation of aminobenzimidazole derivatives with a phenylcyclohexyl acetic acid group as anti-obesity and anti-diabetic agents. Bioorg. Med. Chem. Let. 23 (2013) 4713-4718.

19. T. R. Chen, Luminescence and electroluminescence of bis (2-(benzimidazol-2-yl) quinolinato) zinc. Exciplex formation and energy transfer in mixed film of bis (2-(benzimidazol-2-yl) quinolinato) zinc and N, N′-bis-(1-naphthyl)-N, N′-diphenyl-1, 1′-biphenyl-4, 4′-diamine, J. Mol. Struct. 737 (2005) 35-41.

20. M. Hranjec, E. Horak, M. Tireli, G. Pavlovic, G. Karminski-Zamola, Synthesis, crystal structure and spectroscopic study of novel benzimidazoles and benzimidazo [1, 2-a] quinolines as potential chemosensors for different cations, Dyes Pigm. 95 (2012) 644-656.

21. E. Horak, P. Kassal, M. Hranjec, I. M. Steinberg, Benzimidazole functionalised Schiff bases: novel pH sensitive fluorescence turn-on chromoionophores for ion-selective optodes, Sensor Actuat. B-Chem. 258 (2018) 415-423.

22. A. P. Kulkarni, C. J. Tonzola, A. Babel, S. A. Jenekhe, Electron transport materials for organic light-emitting diodes, Chem. Mater. 16 (2004) 4556-4573.

23. N. Deshapande, N. S. Belavagi, M. G. Sunagar, S. Gaonkar, G. H. Pujar, M. N. Wari, S. R. Inamdar, I. A. M. Khazi, Synthesis, characterization and optoelectronic investigations of bithiophene substituted 1, 3, 4-oxadiazole derivatives as green fluorescent materials. RSC Adv. 5 (2015) 86685-86696.

24. X. Chen, H. Yang, Y. Ge, L. Feng, J. Jia, J. Wang, Synthesis, X- ray crystal structure and optical properties of novel 2- aryl- 3- ethoxycarbonyl- 4- phenylpyrido [1,2- *a*] benzimidazoles, Luminescence. 27 (2012) 382-389.

25. S. H. Cheng, S. H. Chou, W. Y. Hung, H. W. You, Y. M. Chen, A. Chaskar, Y. H. Liu, K. T. Wong, Fine-tuning the balance between carbazole and oxadiazole units in bipolar hosts to realize highly efficient green PhOLEDs, Org. Electron. 14 (2013) 1086-1093.

26. M. Bouchouit, M. E. Said, M. K. Ali, S. Bouacida, H. Merazig, N. K. Chaouche, A. Chibani, B. Zouchoune, A. Belfaitah, A. Bouraiou, Synthesis, X-ray structure, theoretical investigation, corrosion inhibition and antimicrobial activity of benzimidazole thioether and theirs metal complexes, Polyhedron. 119 (2016) 248-259.

27. J. F. Xiong, J. X. Li, G. Z. Mo, J. P. Huo, J. Y. Liu, X. Y. Chen, Z. Y. Wang, Benzimidazole derivatives: selective fluorescent chemosensors for the picogram detection of picric acid, J. Org. Chem. 79 (2014) 11619-11630.

28. C. H. Chen, W. S. Huang, M. Y. Lai, W. C. Tsao, J. T. Lin, Y. H. Wu, T. H. Ke, L. Y. Chen, C. C. Wu, Versatile, Benzimidazole/Amine- Based Ambipolar Compounds for Electroluminescent Applications: Single- Layer, Blue, Fluorescent OLEDs, Hosts for Single-Layer, Phosphorescent OLEDs, Adv. Funct. 19 (2009) 2661-2670.

29. F. D. Lewis, J. L. Hougland, S. A. Markarian, Formation and Anomalous Behavior of Aminonaphthalene− Cinnamonitrile Exciplexes, J. Phys. Chem. A 104 (2000) 3261-3268.

30. Rigaku CrystalClear SM Expert 2.0 r15. Software for data collection and processing, Rigaku Corporation, Tokyo, Japan, 2011.

31. G. M. Sheldrick, A short history of SHELX, Acta Cryst. A 64 (2008) 112-122.

32. A. L. Spek, Structure validation in chemical crystallography, Acta Crystallogr. Sect. D Biol. Crystallogr. 65 (2009) 148-155.

33. C. F. Macrae, I. J. Bruno, J. A. Chisholm, P. R. Edging-ton, P. McCabe, E. Pidcock, L. Rodriguez-Monge, R. Taylor, J. van de Streek, P. A. Wood, Mercury CSD 2.0 – new features for the visualization and investigation of crystal structures, J. Appl. Crystallogr. 41 (2008) 466-470.

34. K. Vasantha, G. Basavarajaswamy, M. V. Rai, P. Boja, V. R. Pai, N. Shruthi, M. Bhat, Rapid ‘one-pot’ synthesis of a novel benzimidazole-5-carboxylate and its hydrazone derivatives as potential anti-inflammatory and antimicrobial agents, Bioorg. Med. Chem. 25 (2015) 1420-1426.

35. M. Barwiolek, A. Wojtczak, A. Kozakiewicz, M. Babinska, A. Tafelska-Kaczmarek, The synthesis, characterization and fluorescence properties of new benzimidazole derivatives, J. Lumin. 211 (2019) 88-95.

36. J. Jayabharathi, V. Thanikachalam, K. Jayamoorthy, Synthesis of some fluorescent benzimidazole derivatives using cobalt (II) hydroxide as highly efficient catalyst–spectral and physico-chemical studies and ESIPT process. Photochem. Photobiol. Sci. 12 (2013) 1761-1773.

37. A. Douhal, F. Amat-Guerri, M. P. Lillo, A. U. Acuna, Proton transfer spectroscopy of 2-(2'-hydroxyphenyl) imidazole and 2-(2'-hydroxyphenyl) benzimidazole dyes. J. Photochem. Photobiol. A. 78 (1994) 127-138.

38. P. Majumdar, J. Zhao, 2-(2-hydroxyphenyl)-benzothiazole (HBT)-rhodamine dyad: acid-switchable absorption and fluorescence of excited-state intramolecular proton transfer (ESIPT). J. Phys. Chem. B. 119 (2015) 2384-2394.

39. V. S. Padalkar, A. Tathe, V. D. Gupta, V. S. Patil, K. Phatangare, N. Sekar, Synthesis and photo-physical characteristics of ESIPT inspired 2-substituted benzimidazole, benzoxazole and benzothiazole fluorescent derivatives. J. Fluoresc. 22 (2012) 311-322.

40. F. A. Chipem, N. Dash, G. Krishnamoorthy, Role of nitrogen substitution in phenyl ring on excited state intramolecular proton transfer and rotamerism of 2-(2′-hydroxyphenyl) benzimidazole: A theoretical study. J. **Chem.** Phys. 134 (2011) 104308.

41. K. Das, N. Sarkar, D. Majumdar, K. Bhattacharyya, Excited-state intramolecular proton transfer and rotamerism of 2-(2′-hydroxyphenyl) benzimidazole. Chem. Phys. Lett. 198 (1992) 443-448.

42. S. K. Behera, G. Sadhuragiri, P. Elumalai, M. Sathiyendiran, G. Krishnamoorthy, Exclusive excited state intramolecular proton transfer from a 2-(2′-hydroxyphenyl) benzimidazole derivative. RSC Adv. 6 (2016) 59708-59717.

43. M. Hranjec, E. Horak, D. Babic, S. Plavljanin, Z. Srdovic, I. M. Steinberg, R. Vianello, N. Perin, Fluorescent benzimidazo [1, 2-a] quinolines: synthesis, spectroscopic and computational studies of protonation equilibria and metal ion sensitivity, New J. Chem. 41 (2017) 358-371.

44. T. Zhang, R. Zhang, Y. Zhao, Z. Ni, A new series of N-substituted tetraphenylethene-based benzimidazoles: Aggregation-induced emission, fast-reversible mechanochromism and blue electroluminescence, Dyes Pigm. 148 (2018) 276-285.

45. D. C. Hu, C. H. Xiao, G. Z. Guo, Y. X. Yang, J. C. Liu, A one-dimensional silver (I) coordination polymer based on the 2-[2-(pyridin-4-yl)-1H-benzimidazol-1-ylmethyl] phenol ligand exhibiting photoluminescence, Acta Crystallogr. E 69 (2013) 356-359.

46. X. Ban, W. Jiang, K. Sun, X. Xie, L. Peng, H. Dong, Y. Sun, B. Huang, L. Duan, Y. Qiu, Bipolar host with multielectron transport benzimidazole units for low operating voltage and high power efficiency solution-processed phosphorescent OLEDs, ACS Appl. Mater. Interfaces. 7 (2015) 7303-7314.

47. S. Xue, X. Qiu, Q. Sun, W. Yang, Alkyl length effects on solid-state fluorescence and mechanochromic behavior of small organic luminophores, J. Mater. Chem. 4 (2016) 1568-1578.

48. D. Ades, V. Boucard, E. Cloutet, A. Siove, C. Olivero, M. C. Castex, G. Pichler, Photoluminescence of donor–acceptor carbazole-based molecules in amorphous and powder forms, J. Appl. Phys. 87 (2000) 7290-7293.

49. E. Ermis, Synthesis, spectroscopic characterization and DFT calculations of novel Schiff base containing thiophene ring, J. Mol. Struct. 1156 (2018) 91-104.

50. H. Bhakhoa, L. Rhyman, P. Ramasami, Theoretical study of the molecular aspect of the suspected novichok agent A234 of the Skripal poisoning, R. Soc. Open Sci. 6 (2019) 181831.

51. C. Y. Panicker, H. T. Varghese, B. Narayana, K. Divya, B. K. Sarojini, J. A. War, C. Van Alsenoy, H. K. Fun, FT-IR, NBO, HOMO–LUMO, MEP analysis and molecular docking study of Methyl N-({[2-(2-methoxyacetamido)-4-(phenylsulfanyl) phenyl] amino}[(methoxycarbonyl) imino] methyl) carbamate, Spectrochim. Acta A 148 (2015) 29-42.